CFD analysis of delayed ignition hydrogen releases from a train inside a tunnel

Tolias, I.C.[1], Rattigan, W.[2], Lyons, K.[2], Koumroglou, V.C.[3], Venetsanos, A.G.[1]
[1] Environmental Research Laboratory, INRASTES, National Centre for Scientific Research Demokritos, Patriarchou Grigoriou E & 27 Neapoleos Str., 15341, Agia Paraskevi, Greece, tolias@ipta.demokritos.gr
[2] HSE Science and Research Centre, Buxton, United Kingdom, Wayne.Rattigan@hse.gov.uk, Kieran.Lyons@hse.gov.uk
[3] Core department, National and Kapodistrian University of Athens, Euripus Campus GR 34400, Greece vkoumr@gmail.com

ABSTRACT

In the present work, we present the results of numerical simulations involving the dispersion and combustion of a hydrogen cloud released in an empty tunnel. The simulations were conducted with the use of ADREA-HF CFD code and the results are compared with measurements from experiments conducted by HSE in a tunnel with the exact same geometry. The length of the tunnel is equal to 70 m and the maximum height from the floor is equal to 3.25 m. Hydrogen release is considered to occur from a train containing pressurized hydrogen stored at 580 bars. The release diameter is equal to 4.7 mm and the release direction is upwards. Initially, dispersion simulation was performed in order to define the initial conditions for the deflagration simulations. The effect of the initial wind speed and the effect of the ignition delay time were investigated. An extensive grid sensitivity study was conducted in order to achieve grid independent results. The CFD model takes into account the flame instabilities that are developed as the flame propagates inside the tunnel and turbulence that exists in front of the flame front. Pressure predictions are compared against experimental measurements revealing a very good performance of the CFD model.

Keywords: Hydrogen deflagration, CFD, Modelling, Tunnel, wind effect, ignition delay

1.0 INTRODUCTION

Hydrogen use is expected to increase in the near future and its explosive nature brings up significant safety issues. In the case of an accident, hydrogen mixes with air and forms a flammable cloud. An accidental release in closed space can have catastrophic consequences in the case of an explosion. The confined space will lead to the development of much higher over-pressure compared to a similar explosion in open space.

In the past years, the increase of computational power has rendered Computational Fluid Dynamics (CFD) as a very attractive methodology for risk assessment. CFD can lead to evaluation of existing regulations and standards and at the same time give deeper insight into the physical phenomenon. CFD modeling of deflagrations is a big challenge. Combustion occurs at very small scales of the order of millimeters whereas geometries of practice interest are of order of meters. The growth of instabilities at the flame front, the complex interaction between the flame and the turbulence along with the very wide range of applications, make the development of a global model a difficult task.

Many numerical studies that include hydrogen dispersion from a vehicle can be found in the literature. Venetsanos et al. [1] studied with the use of Computational Fluid Dynamics (CFD) an accident that happened in Stockholm at 1983 after the release of approximately 13.5 kg of hydrogen from a rack of 18 interconnected pressure vessels on a delivery truck. Later studies included hydrogen dispersion at various locations such as inside a tunnel [2], in a refuelling station [3], inside a garage [4] and in an underpass [5]. Middha and Hansen [6] investigated with CFD the risk from hydrogen vehicles in tunnels, for various scenarios including car and bus accidents in horse-shoe tunnels for a mix of longitudinal ventilation speeds. Houf et al [7] examined with CFD a release of a total of 5 kg of

hydrogen from three 700-bar tanks in a transversely-ventilated tunnel. More recently, Li and Luo [8] examined the dispersion around a car in the open atmosphere due to a downwards hydrogen leakage from a Thermally activated Pressure Relief Device (TPRD) of 4.2 mm. Hussein et al. [9] investigated various hydrogen release scenarios from cars in a naturally ventilated car park. They considered a 700 bar tank, TPRD sizes between 0.5 mm and 3.34 mm and downward release angles of 0, 30 and 45 degrees. An independent but similar study was performed from Shentsov et al. [10]. They examined releases from TPRDs of 0.5-2 mm, various ventilation strengths and release directions. The dispersion of hydrogen in an open garage was also studied by Lv et al. [11] and Shen et al. [12] across various parking scenarios. They specifically examined the effects of upward and downward releases from TPRDs of 2-4 mm of a 700 bar tank.

In the current work, experiments that were recently performed by HSE in a model of a tunnel were simulated using CFD. The objective of the study is to verify the accuracy of our CFD model, analyze the experiments to gain a deeper understanding of the phenomena and investigate the impact of certain parameters, such as wind and ignition delay, on the results.

2.0 DESCRIPTION OF EXPERIMENTS

Hydrogen dispersion and deflagration experiments of hydrogen released from a train inside tunnel model were conducted by HSE. The length of the tunnel is equal to 70 m and the maximum height from the floor equal to 3.25 m. The hydrogen mass is equal to 5.55 kg stored at 580 bars. The release diameter is equal to 4.7 mm and the release direction is upwards. Release is located at x=35, y=0.6, z=1.54 m (reference point is at tunnel entrance, in the middle of the tunnel floor). The ignition position in ignited tests is positioned at x=38, y=0.6, z=2.95 m. Once igniter is activated a spark exists continuously.

Tests that are studied in the present work (referenced by the experimentalists as “Train2”) are presented in Table 1. These tests do not include the train obstacle (empty tunnel cases). Forced ventilation from the one opening of the tunnel is used in Test 6 and 25 whereas natural ventilation due to meteorological conditions exists in Tests 55, 56, 57. It is important to mention that hydrogen concentrations were exclusively measured in cases where ignition did not occur (that is Test 6). Thus, test number 6 is used to validate hydrogen concentration from dispersion simulations which are important because it defines the initial conditions for the deflagration simulations. Table 1 demonstrates that the ignited case (Test 25) exhibit some differences in wind speed when compared to the unignited one (Test 6). These differences arise from variations in meteorological conditions (wind speed) which affect the ventilation system. We should note that in Tests 55-57 the presented wind range due to the natural ventilation was measured inside the tunnel prior to hydrogen release. Consequently, wind speed could be different during the experiment. Finally, in Test 55, the igniter was activated before hydrogen release and therefore the ignition took place once the flammable gas cloud reached the igniter location (this is why the ignition delay is equal to zero in Table 1).

Table 1. Examined experimental cases of “Train2” scenarios

Test Number	Ignited	Ignition delay	Congestion	Wind type	Wind range
6	No	–	No	Forced ventilation	0.8 – 1.5
25	Yes	8.5 s	No	Forced ventilation	1.0 – 1.6
55	Yes	0.0 s	No	Natural ventilation	1.5 – 1.9*
56	Yes	1.8 s	No	Natural ventilation	1.5 – 1.9*
57	Yes	6.5 s	No	Natural ventilation	1.5 – 1.9*

3.0 NUMERICAL MODELLING

3.1 Governing equations - Combustion model

For the CFD simulations the ADREA_HF code was used [13][14]. The model solves the ensemble-averaged continuity equation, the Navier-Stokes equations, the energy equation (conservation equation of total enthalpy) and the conservation equation of hydrogen, oxygen and water mass fraction (one step irreversible reaction equation for hydrogen combustion is used). The multi-component mixture is assumed to be in thermodynamic equilibrium. The ideal gas equation of state is used. Turbulence is modelled using the URANS (Unsteady Reynolds averaged Navier-Stokes equations) approach and the Kato and Launder modification of the k-ε model was used [15]. The Birch 84 [16] notional approach was employed to model the under-expanded jet and to estimate the conditions after the jet has expanded to ambient pressure. The notional conditions are set as hydrogen release conditions in the CFD simulation.

The combustion model that we developed and validate in [17][18][19] is used and is described briefly in next. The reaction rate for hydrogen which appears in its conservation equation is modelled based on the turbulent burning velocity (S_T) concept [20]:

$$\overline{R}_f = \rho_u S_T \left| \nabla q_f \right| \tag{1}$$

where q_f is the fuel mass fraction and ρ_u is the density in the unburned region which is estimated using the assumption of adiabatic compression. The turbulent burning velocity is modelled considering all the main factors that affect the total reaction rate: laminar burning velocity, turbulence existing in front of the flame front, hydrodynamic instability and non-equidiffusive effects. It is estimated from the relations:

$$S_T' = S_L + u'\left(1 + Da^{-2}\right)^{-1/4} \tag{2}$$

$$S_T = \Xi_k \cdot \Xi_{lp} \cdot S_T' \tag{3}$$

In these equations, S_T is the turbulent burning velocity, S_T' the intermediate turbulent burning velocity which accounts only for the turbulence that exists in front of the flame front (Schmid's relation [21]), S_L the laminar burning velocity (function of pressure and local mixture composition), Da the Damköhler number, u' is the rms (root mean square) of velocity fluctuations and Ξ are factors that account for unresolved phenomena which accelerate the combustion process. The above formulation of the combustion model considers that the modelled phenomena are independent from each other and thus to wrinkle the flame at different scales [17]. We should note that as u' goes to zero, S_T goes to $S_L^{sgs} = \Xi_k \cdot \Xi_{lp} \cdot S_L$.

Ξ_k accounts for turbulence that is generated by the flame front itself. This phenomenon is driven by the hydrodynamic instability, and as a result Ξ_k depends on the expansion coefficient E. Hydrodynamic instability needs some distance, R_0 , in order to be fully developed. In order to account for the transient stage, Ξ_k is estimated from the relation $\Xi_k = 1 + \left(\psi \cdot \Xi_k^{\max} - 1\right) \cdot \left[1 - \exp\left(-R/R_0\right)\right]$ [22][23] where R is the distance from the ignition point and $\Xi_k^{\max} = \left(E - 1\right)/\sqrt{3}$ [24]. ψ is a model constant varying between 0 and 1 which represents the level at which the maximum value $\Xi_k^{\max}$ is reached. The value of 0.5 was used in this study.

Ξ_{lp} accounts for non-equidiffusive effects. In lean hydrogen mixtures, non-equidiffusive effects make the flame unstable wrinkling its surface and increasing the combustion rate [25]. This instability, which is often called diffusional-thermal, develops faster than the hydrodynamic one and thus it influences the deflagration process at the very early stages [26]. Ξ_{lp} increases linearly from the value of one to a constant maximum value at a given distance where the instability is considered to be fully developed. This distance is set equal to 0.1 m based on the experimental data of Kim et al. [26]. The maximum value of Ξ_{lp} can be estimated [27] based on the leading point concept of Zimont and Lipatnikov work [28]. For 18% hydrogen concentration, it is approximately equal to 2. The fact that the effect of diffusional-thermal instability can be modelled by increasing the burning velocity by a constant factor is supported by the work of Bauwens et al. [29][30].

3.2 Numerical details

In dispersion simulations, the domain covers the area from x=0 m (tunnel entrance) to x=120 m (50 m away from tunnel exit) in the horizontal direction, from y=-25 m to y=25 m in the lateral and from z=0 m to z=14 m in the vertical direction. At the entrance of the tunnel constant horizontal velocity was applied to model the ventilation. In deflagration simulations the domain is expanded also before the entrance of the tunnel by 50 m. The top and the sides of the tunnel were blocked with obstacles in order to reduce the number of active cells and save computational time (Figure 1). The computational grid details are presented in the grid independency study section.

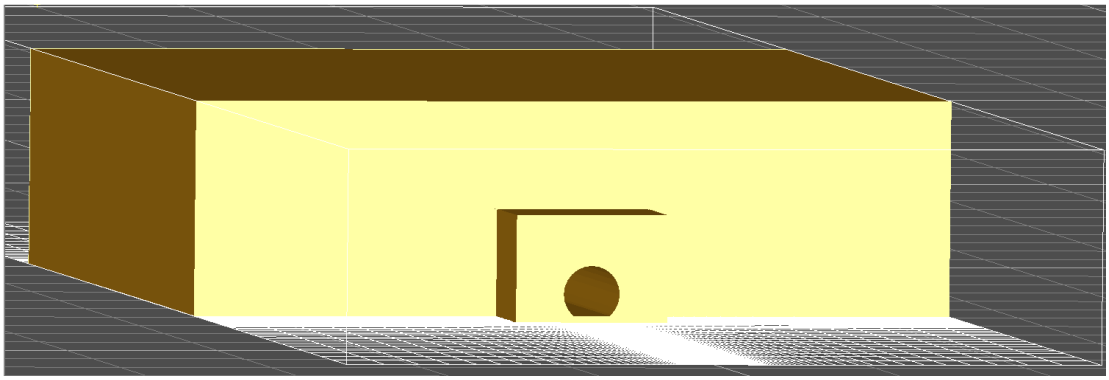

Figure 1. Geometry at the exit of the tunnel and part of the domain.

ADREA-HF uses the finite volume method on a staggered Cartesian grid. The pressure and velocity equations are decoupled using a modification of the SIMPLER algorithm. For the discretization of the convective terms the bounded second order upwind method is used [31]. For time advancement, the fully implicit first order accurate scheme was chosen. Time step is automatically adapted according to desired Courant–Friedrichs–Lewy (CFL) number which was set equal to 10 in dispersion simulations and equal to 0.1 in deflagration simulations. Ignition is modelled by fixing the reaction rate in a cell at the ignition point, in order the initial amount of fuel to be burned in 3.6 ms. This time was estimated based on laminar flame velocity and cell size at the ignition point for the grid independent grid.

4.0 RESULTS AND DISCUSSION

4.1 Grid independence study

In order to assess grid independency many different grids were examined. For every grid all the stages were simulated: initial velocity field, dispersion stage, deflagration stage. Ventilation equal to 1.3 m/s was considered (average of the measured range in Test 26).

In Table 2 details of the grids that were used are presented. Preliminary simulations revealed that the number of cells in the x direction at the area where hydrogen is mainly accumulated (between x=35 m

and x=55 m) is very important for achieving grid-independent results, especially for the deflagration simulations. Consequently, to examine the effect in overpressure, four grids with different number of cells only in the x direction are used (Grids 1 to 4 in Table 2). Then, in order to examine the effect of the number of cells in y and z directions, two additional grids were utilized (Grids 5 and 6 in Table 2). In these grids an increased number of cells in y and z direction were used. Grid 5 and Grid 6 has the same number of cells in x direction with Grid 2 and Grid 4 respectively.

The total number of active cells presented in Table 2 is higher than the product of the number of cells in each direction because block areas with obstacles exists outside the tunnel (at the top and the sides of the tunnel) in order to save computational time. The number of cells in each direction corresponds to those of the entire domain. In denser grids, the number of cells in y and z direction is increased mainly inside the tunnel (not in the grid expansions outside of it). In the x direction, the number of cells is increased mainly at the area between the jet release (35 m) and the point of approximately 55 m. In this length the main volume of hydrogen in accumulated due to the effect of the initial flow field. In Grid 6, the number of cells outside the tunnel in x, y, z directions are 41, 64 and 29 respectively. In other grids the numbers are similar.

Table 2. Grid characteristics

Grid cases					
ID	Name	Number of cells in x direction	Number of cells in y direction	Number of cells in z direction	Total number of active cells
1	Grid_1x_1yz	**288**	117	94	1,242,886
2	Grid_2x_1yz	**490**	117	94	1,821,909
3	Grid_3x_1yz	**646**	117	94	2,268,849
4	Grid_4x_1yz	**788**	117	94	2,679,705
5	Grid_2x_2yz	490	**144**	**114**	3,024,893
6	Grid_3x_2yz	646	**144**	**114**	3,804,269

In Figure 2 the grid independency study for the first 4 grids are presented. These grids differ only in the number of cells in x direction. Overpressure time series are presented in two positions, one near the ignition point and one away from it. We observe that initial grids exhibit differences in maximum overpressure. Only the two densest grids (Grid_3x_1yz and Grid_4x_1yz) achieve the same overpressure values.

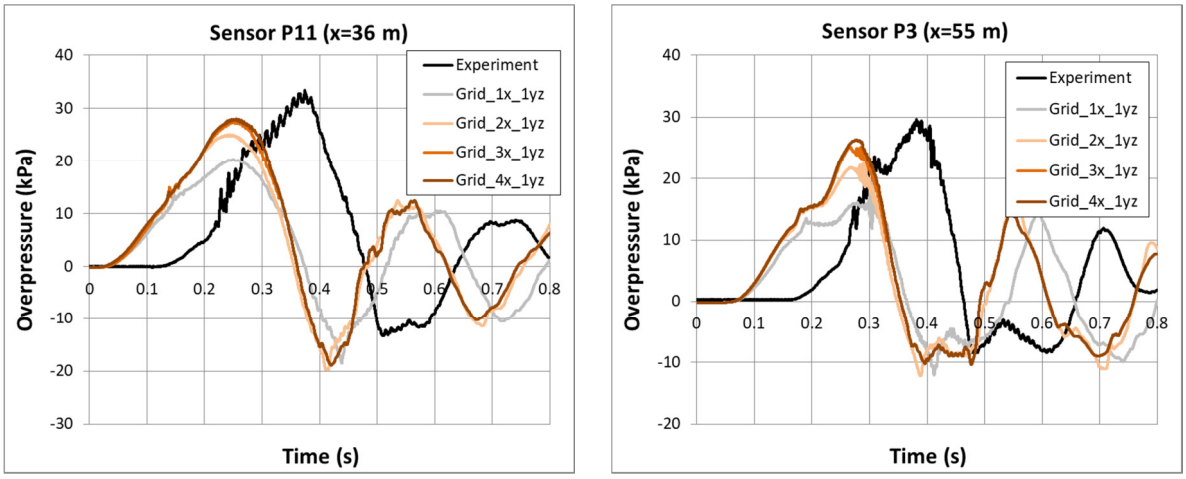

Figure 2. Effect of grids with different number of cells in x direction. Overpressure time series at two sensors.

In Figure 3 the grid independency study is presented regarding the number of cells in y, z directions. Grid_2x_1yz and Grid_2x_2yz (continuous and dashed lines respectively) have the same number of

cells in x direction and differs in the number of cells in y, z direction. We observe that differences in maximum overpressure exist. Grid_3x_1yz and Grid_3x_2yz compares again grids with different number of cells in y, z directions but this time using denser grid in x direction. We observe that the differences between the results are similar. Denser grids in y and z directions were not tested due to prohibited large computational times.

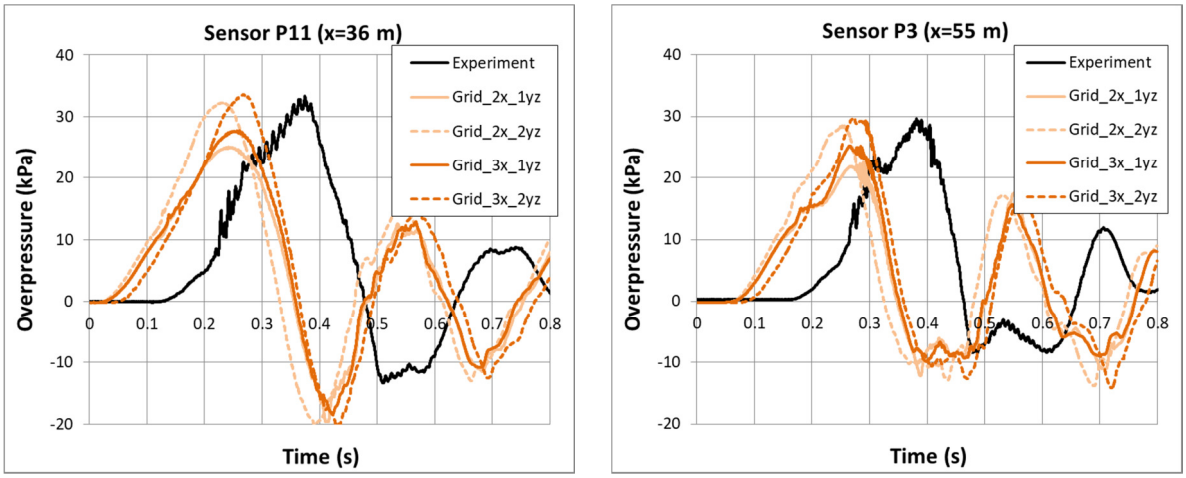

Figure 3. Effect of grids with different number of cells in y, z direction. Overpressure time series at two sensors.

Figure 4 presents hydrogen volume concentration at the time of the ignition (8.5 s after the start of the release) for different grids. We observe that Grid_1x_1yz has negligible differences compare with Grid_2x_1yz. However, the difference in maximum overpressure is significant (Figure 2). The differences in hydrogen concentration between Grid_2x_1yz and Grid_3x_1yz are negligible again but differences in maximum overpressure still exist (Figure 2). These results indicate that the results from the dispersion simulations (which are used to calculate hydrogen concentrations) were grid independent. As a result grid independency was not achieved in overpressure because denser grids in x directions are needed in deflagration simulation. Finally, Grid_3x_1yz and Grid_4x_1yz exhibit minor differences in hydrogen concentration. This time the differences in overpressure time series are minor as well (Figure 2).

Grid_2x_1yz and Grid_2x_2yz have the same number of cells in x direction and differ in the number of cells in y, z direction. Hydrogen concentrations have some differences mainly around x=43 m. Overpressure time series have differences as well with the denser grid achieving higher maximum overpressure (Figure 3). Similar conclusions are made comparing Grid_3x_1yz and Grid_3x_2yz which also differs only in the number of cells in y, z direction.

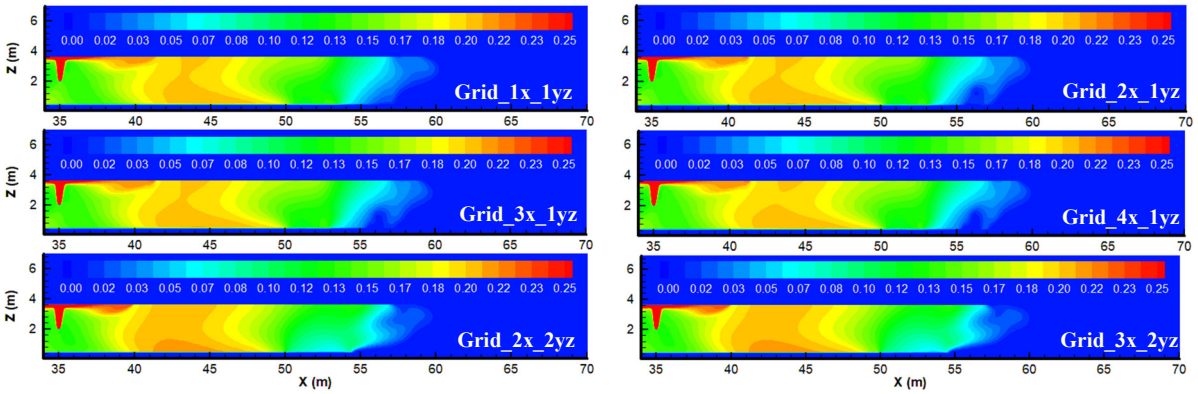

Figure 4. Hydrogen volume concentration at the time of ignition (8.5 s after the start of the release) for different grids (Table 2)

The above analysis indicates that grid independency is achieved in x direction whereas denser grids need to be tested in other directions in order to ensure grid independence. The densest grid Grid_3x_2yz is used in the rest of the sections.

4.2 Flame propagation

In Figure 5 flame propagation is indicated by hydrogen volume concentration contours. As the combustion progresses a velocity field is developed due to the expansion of combustion products which pushes the hydrogen-air mixture towards the exits of the tunnel. At t=0.26 s the flame front contacts the ground. Around this time the maximum overpressure occurs (Figure 3). We observe that at this time a large volume of unburned hydrogen exists. Consequently this volume does not contribute to maximum overpressure. The maximum hydrogen concentrations away from the jet area are around 20-22%. These values are located initially at the area between x=40 and x=46 m. We observe that at the time of 0.26 s only the half of the 20-22% concentration area has been consumed. It seems that only the hydrogen that exists in 5 m radius from the ignition point contributes to maximum overpressure. This radius is equal to 1.5 times the tunnel height.

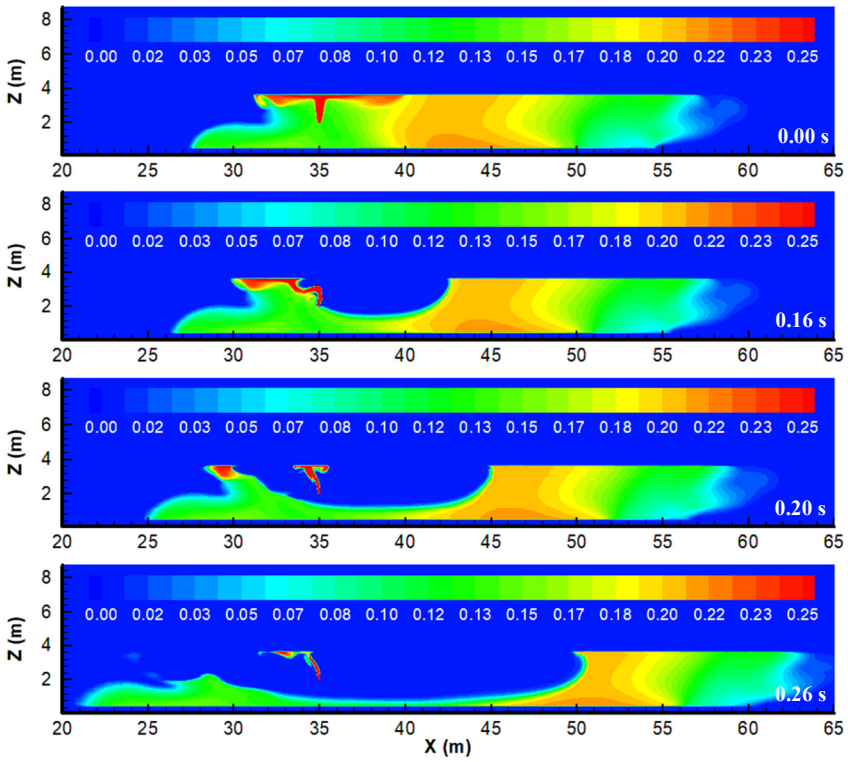

Figure 5. Flame propagation: hydrogen volume concentration at 0.00, 0.16, 0.20, 0.26 s after the ignition. Ignition is located near the ceiling at x=38 m.

4.3 Wind effect

In Figure 6 the hydrogen volume concentration contours are presented at 8.5 s (ignition time) for 1.0, 1.3 and 1.6 m/s wind speed. We observe that wind has a significant effect of hydrogen cloud. Higher wind speeds lower the maximum concentration but also lead to bigger clouds which spread to a greater distance downwind the release.

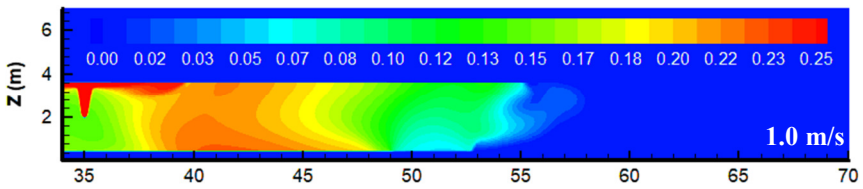

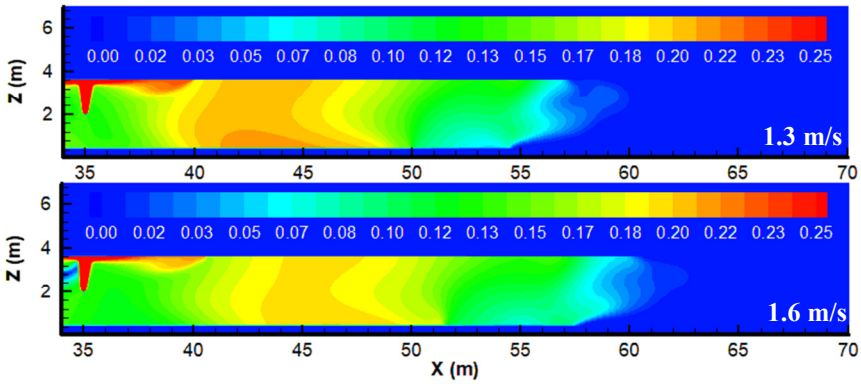

Figure 6. Hydrogen volume concentration at the time of ignition (8.5 s after the start of the release) for different inlet wind speed: 1.0 m/s (top), 1.3 m/s (middle) and 1.6 m/s (bottom). Wind blows from the left.

Hydrogen volume concentration at several points inside the tunnel downwind the release (which is located at x=35, y=0.6, z=1.54 m) are presented in Figure 7 for the three different inlet wind speeds. Even though in the unignited experiment the maximum value of the wind speed is 1.5 (Test 6, Table 1), the value of 1.6 is also tested because this is the maximum value in the ignited case (Test 25). The first row corresponds to positions at 2.8 m height from the ground, the second at 1.7 m and the third at 0.5 or 1.0 m. In most sensors a time difference is observed between experimental and computational results. We should note that the experimental time has low accuracy because of the way that the measurements were made. As a result the comparison should be focused on the general trend of the curves and the maximum values.

The trend of the experimental curves is predicted satisfactory in most of the sensors. Maximum values are predicted more accurate by the wind cases of 1.0 or 1.3 m/s. In sensors 3 the simulations exhibits the highest deviation from the experimental results. This sensor is located near the release point at the ground level.

Comparing the results from the different wind speeds, differences are observed approximately after 4 s. At the initial times hydrogen flow rate is very high and as a result dominates the flow field reducing the effect of wind speed. However at higher times the flow rate has decreased due to blowdown and hydrogen has also moved away from the release making the effect of wind more prominent. The time of 8.5 s when ignition is occurred is highlighted in the plots. In all sensors, after some time the higher the wind is the lower the concentrations are. Higher wind speed leads to more fresh air which mixes with hydrogen lowering the concentration. This is also indicated in the contours in Figure 6.

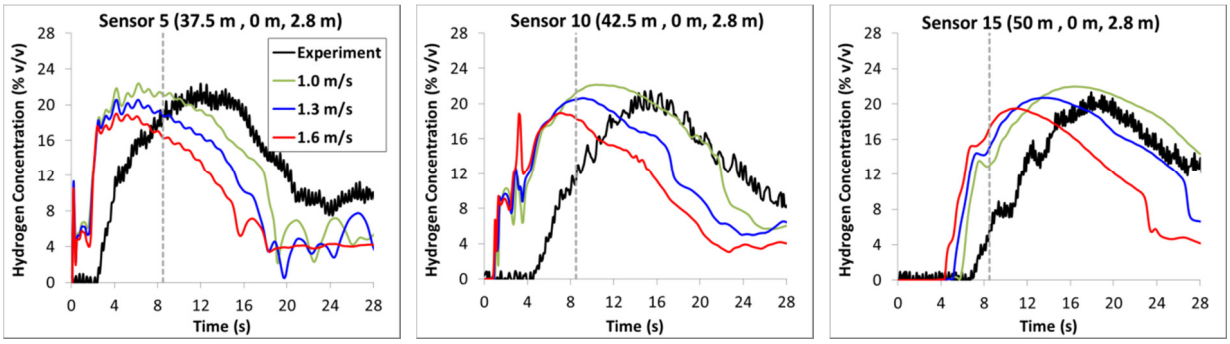

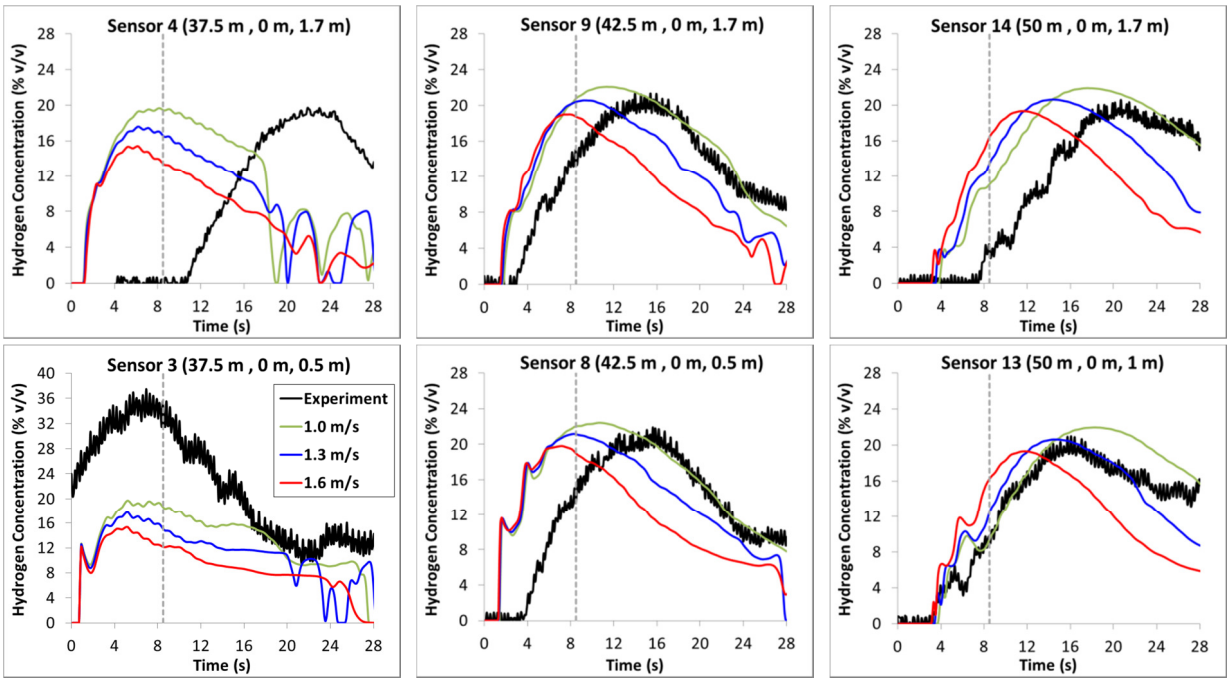

Figure 7. Hydrogen volume concentration. Comparison of experimental and computational results for three different inlet wind speeds. Release is located at x=35, y=0.6, z=1.54 m. Experimental wind speed varies in the range 0.8 – 1.5 m/s. Time of ignition is highlighted with dashed vertical line.

In Figure 8 the effect of wind speed on overpressure is presented. We observe that the effect is significant. The lowest wind speed achieves the highest overpressure whereas the highest wind speed achieves the lowest overpressure. This behavior is explained by the different concentrations fields at the time of ignition (Figure 6, Figure 7). Higher wind speeds decrease the maximum concentrations which contribute the most in overpressure development. Moreover, as it is shown in Figure 6 the higher wind moves the high concentration area of the cloud away from the ignition point (which is located near the ceiling at x=38 m). This is also responsible for the lower overpressure values.

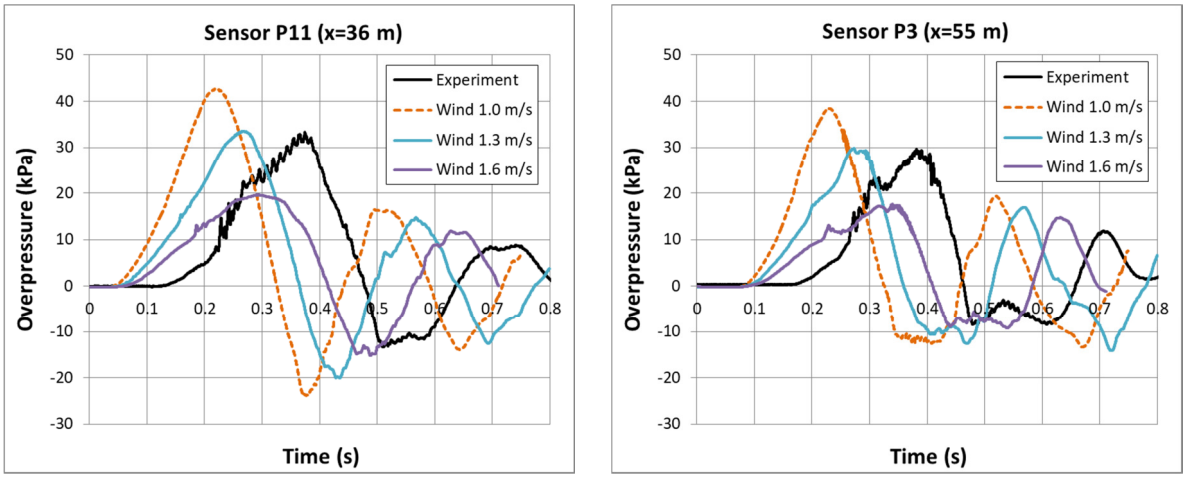

Figure 8. Effect of wind speed in overpressure.

4.4 Ignition delay

The effect of ignition delay on overpressure is presented in Figure 9 for the experiment (Test 55, 56, 57) and the simulations. In these experiments, no forced ventilation was used. Initial wind exists inside the tunnel due to the meteorological conditions. The initial wind was measured prior to the

experiments and it was found to be in the range 1.5 – 1.9 m/s (Table 1). Thus, wind speed equal to 1.7 m/s are used in simulations. In ignition delay 6.5 s case wind speed equal to 1.0 s is also tested.

We observe that the agreement between simulation and experiment in the 1.8 and 0.0 s ignition delay cases are very satisfactory. Maximum overpressure is predicted accurately enough. On the other hand, the case of 6.5 s (wind 1.7 m/s) presents significant differences compared to the experiment. The predicted maximum overpressure is approximately half the experimental one. The agreement improves significantly when a lower wind speed is used (1.0 m/s). We observe that wind speed has a significant impact on overpressure, similarly to the case of 8.5 s ignition delay (Section 4.3). Consequently, a possible reason for the differences in 6.5 s case is that wind due to meteorological conditions during hydrogen release to be lower than the measured ranged before the release. We expect that the effect of wind to be less evident in lower ignition delay time (0.0 s and 1.8 s case) compared to the higher one (see also Section 4.3).

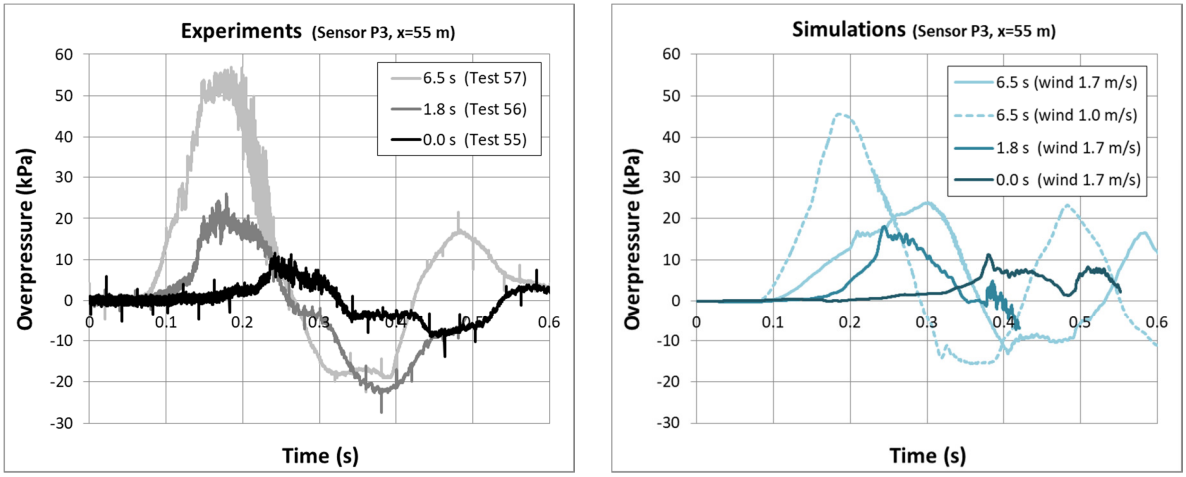

Figure 9. Effect of ignition delay in overpressure at sensor P3 (x=55 m) in experiments (left) and simulations (right).

5.0 CONCLUSIONS

Hydrogen dispersion and deflagration experiments that were recently performed by HSE in a model of a tunnel were simulated using the ADREA-HF CFD code. A detailed grid independency study was conducted revealing that deflagrations results are particular sensitive to grid changes in the x-direction. Grid independency was achieved in x-direction by using a high number of cells in order to resolve with accuracy the flame front at the area where hydrogen is mainly accumulated. Denser grids need to be tested in other directions in order to ensure grid independence in these directions too.

The agreement between simulation results and measurements was very good in the forced ventilation case. Simulation results reveal that only the hydrogen that exists in 5 m radius from the ignition point contributes to maximum overpressure. This radius is equal to 1.5 times the tunnel height.

The wind effect was studied showing that even small changes in wind can have significant changes in overpressure. High wind values decrease hydrogen concentrations and also moves the high concentration area of the cloud away from the ignition point. These result in lower overpressures. About the experiments with different ignition delay, good agreement is achieved in the 0.0 s and 1.8 s cases. In the 6.5 s case the overpressure is predicted better when using wind speed equal to 1.0 m/s rather than the measured (prior to the experiment) speed of 1.7 m/s.

As future work, the effect of a variable wind speed model at the tunnel entrance could be examined in order to reproduce the experimental conditions better. Moreover, the effect of ignition delay could be

studied using several initial wind speeds. Finally, the experimental cases with the train obstacle need to be studied in order to evaluate the effect of congestion on the results.

ACKNOWLEDGEMENTS

The research leading to these results was financially supported by the HyTunnel-CS which has received funding from the Fuel Cells and Hydrogen 2 Joint Undertaking under grant agreement No 826193. This Joint Undertaking receives support from the European Union's Horizon 2020 research and innovation programme, Hydrogen Europe and Hydrogen Europe research. The authors would like also to acknowledge the Greek Research & Technology Network (GRNET) for the computational time granted us in the Greek National HPC facility ARIS (http://hpc.grnet.gr) under project H2TUN (pr014025).

REFERENCES

[1] Venetsanos A., Huld T, Adams P, Bartzis J. Source, dispersion and combustion modelling of an accidental release of hydrogen in an urban environment. J Hazard Mater 2003;105:1–25. doi:10.1016/j.jhazmat.2003.05.001.

[2] Venetsanos AG, Baraldi D, Adams P, Heggem PS, Wilkening H. CFD modelling of hydrogen release, dispersion and combustion for automotive scenarios. J Loss Prev Process Ind 2008;21:162–84. doi:10.1016/j.jlp.2007.06.016.

[3] Baraldi D, Venetsanos a. G, Papanikolaou E, Heitsch M, Dallas V. Numerical analysis of release, dispersion and combustion of liquid hydrogen in a mock-up hydrogen refuelling station. J Loss Prev Process Ind 2009;22:303–15. doi:10.1016/j.jlp.2008.10.004.

[4] Papanikolaou EA, Venetsanos AG, Heitsch M, Baraldi D, Huser A, Pujol J, et al. HySafe SBEP-V20: Numerical studies of release experiments inside a naturally ventilated residential garage. Int J Hydrogen Energy 2010;35:4747–57. doi:10.1016/j.ijhydene.2010.02.020.

[5] Venetsanos AG, Papanikolaou E, Hansen OR, Middha P, Garcia J, Heitsch M, et al. HySafe standard benchmark Problem SBEP-V11: Predictions of hydrogen release and dispersion from a CGH2 bus in an underpass. Int J Hydrogen Energy 2010;35:3857–67. doi:10.1016/j.ijhydene.2010.01.034.

[6] Middha P, Hansen OR. CFD simulation study to investigate the risk from hydrogen vehicles in tunnels. Int J Hydrogen Energy 2009;34:5875–86. doi:10.1016/j.ijhydene.2009.02.004.

[7] Houf WG, Evans GH, Merilo E, Groethe M, James SC. Releases from hydrogen fuel-cell vehicles in tunnels. Int J Hydrogen Energy 2012;37:715–9. doi:10.1016/j.ijhydene.2011.09.110.

[8] Li Z, Luo Y. Comparisons of hazard distances and accident durations between hydrogen vehicles and CNG vehicles. Int J Hydrogen Energy 2019;44:8954–9. doi:10.1016/j.ijhydene.2018.07.074.

[9] Hussein H, Brennan S, Molkov V. Dispersion of hydrogen release in a naturally ventilated covered car park. Int J Hydrogen Energy 2020;45:23882–97. doi:10.1016/j.ijhydene.2020.06.194.

[10] Shentsov V, Makarov D, Molkov V. Effect of TPRD diameter and direction of release on hydrogen dispersion in underground parking. 9th nternational Conf. Hydrog. Saf., On-Line Conference: 2021, p. 1627–40.

[11] Lv H, Shen Y, Zheng T, Zhou W, Ming P, Zhang C. Numerical study of hydrogen leakage, diffusion, and combustion in an outdoor parking space under different parking configurations. Renew Sustain Energy Rev 2023;173:113093. doi:10.1016/j.rser.2022.113093.

[12] Shen Y, Zheng T, Lv H, Zhou W, Zhang C. Numerical Simulation of Hydrogen Leakage from Fuel Cell Vehicle in an Outdoor Parking Garage. World Electr Veh J 2021;12:118. doi:10.3390/wevj12030118.

[13] Venetsanos AG, Papanikolaou EA, Bartzis JG. The ADREA-HF CFD code for consequence

assessment of hydrogen applications. Int J Hydrogen Energy 2010;35:3908–18. doi:doi.org/10.1016/j.ijhydene.2010.01.002.

[14] Tolias IC, Venetsanos AG, Markatos N, Kiranoudis CT. CFD modeling of hydrogen deflagration in a tunnel. Int J Hydrogen Energy 2014;39:20538–46. doi:10.1016/j.ijhydene.2014.03.232.

[15] Kato M, Launder BE. The modeling of turbulent flow around stationary and vibrating square cylinders. Ninth Symp. Turbul. Shear Flows, Kyoto, Japan, August 16-18: 1993.

[16] Birch AD, Brown DR, Dodson MG, Swaffield F. The structure and concentration decay of high pressure jets of natural gas. Combust Sci Technol 1984;36:249–61. doi:10.1080/00102208408923739.

[17] Tolias IC, Venetsanos AG. An improved CFD model for vented deflagration simulations – Analysis of a medium-scale hydrogen experiment. Int J Hydrogen Energy 2018;43:23568–84. doi:10.1016/J.IJHYDENE.2018.10.077.

[18] Tolias IC, Venetsanos AG, Kuznetsov M, Koutsoukos S. Evaluation of an improved CFD model against nine vented deflagration experiments. Int J Hydrogen Energy 2020;46:12407–19. doi:10.1016/j.ijhydene.2020.09.231.

[19] Momferatos G, Giannissi SG, Tolias IC, Venetsanos AG, Vlyssides A, Markatos N. Vapor cloud explosions in various types of confined environments: CFD analysis and model validation. J Loss Prev Process Ind 2022;75:104681. doi:10.1016/j.jlp.2021.104681.

[20] Lipatnikov AN, Chomiak J. Turbulent flame speed and thickness: phenomenology, evaluation, and application in multi-dimensional simulations. Prog Energy Combust Sci 2002;28:1–74.

[21] Schmid H-P, Habisreuther P, Leuckel W. A Model for Calculating Heat Release in Premixed Turbulent Flames. Combust Flame 1998;113:79–91. doi:10.1016/S0010-2180(97)00193-4.

[22] Molkov V, Makarov D, Schneider H. LES modelling of an unconfined large-scale hydrogen-air deflagration. J Phys D (Applied Physics) 2006;39:4366–76. doi:10.1088/0022-3727/39/20/012.

[23] Xiao H, Makarov D, Sun J, Molkov V. Experimental and numerical investigation of premixed flame propagation with distorted tulip shape in a closed duct. Combust Flame 2012;159:1523–38. doi:10.1016/j.combustflame.2011.12.003.

[24] Karlovitz B, Denniston DW, Wells FE. Investigation of Turbulent Flames. J Chem Phys 1951;19:541. doi:10.1063/1.1748289.

[25] Jomaas G, Law CK, Bechtold JK. On transition to cellularity in expanding spherical flames. J Fluid Mech 2007;583:1–26. doi:10.1017/S0022112007005885.

[26] Kim WK, Mogi T, Kuwana K, Dobashi R. Self-similar propagation of expanding spherical flames in large scale gas explosions. Proc Combust Inst 2015;35:2051–8. doi:10.1016/j.proci.2014.08.023.

[27] Molkov V. Fundamentals of Hydrogen Safety Engineering, parts I & II. Free download e-book, bookboon.com, ISBN: 978-87-403-0279-0; 2012.

[28] Zimont V, Lipatnikov A. A numerical model of premixed turbulent combustion of gases. Chem Phys Rep 1995;14:993–1025.

[29] Bauwens CR, Dorofeev SB. Effect of initial turbulence on vented explosion overpressures from lean hydrogen–air deflagrations. Int J Hydrogen Energy 2014;39:20509–15. doi:10.1016/j.ijhydene.2014.04.118.

[30] Bauwens CR, Chaffee J, Dorofeev SB. Vented explosion overpressures from combustion of hydrogen and hydrocarbon mixtures. Int J Hydrogen Energy 2011;36:2329–36. doi:10.1016/j.ijhydene.2010.04.005.

[31] Waterson NP, Deconinck H. Design principles for bounded higher-order convection schemes – a unified approach. J Comput Phys 2007;224:182–207. doi:https://doi.org/10.1016/j.jcp.2007.01.021.